Special Issue on Nuclear Science and Technology

ARTICLE

Comparative neutronic performance of UO_2 ceramic and UO_2-silumin fuels in a VVER-1200 reactor using GETERA code

Rolando F. Menor, Jr.*[1] and Rothana S. Hor[2]

[1]Nuclear Reactor Operations Section, Nuclear Services Division, Department of Science and Technology – Philippine Nuclear Research Institute, Philippines, Diliman, Quezon City 1101, Philippines

[2]School of Nuclear Science and Engineering, Tomsk Polytechnic University, Tomsk 634050, Russia

ABSTRACT

Interest in the development of accident-tolerant fuels (ATFs) has intensified significantly, driven by the need to mitigate the high-temperature vulnerabilities of traditional uranium dioxide (UO_2) fuel systems during severe accident scenarios. The objective of this study is to examine the viability of an alternative UO_2-silumin matrix dispersion fuel, inspired by small modular marine reactors, for deployment in a large-scale commercial VVER-1200 pressurized water reactor. To evaluate this advanced fuel system, steady-state core thermal-hydraulic calculations were coupled with neutronic depletion analyses using the deterministic GETERA-93 code. Key operational metrics, including axial temperature profiles, core criticality variations, and spent fuel nuclide evolution, were evaluated relative to a standard UO_2 baseline. The thermal-hydraulic findings revealed that the high thermal conductivity of the UO_2-silumin matrix fuel reduced the peak centerline fuel temperature from 1819.7°C to 526.9°C under nominal full-power conditions, significantly expanding thermal safety margins during severe-accident scenarios. Neutronic optimization results indicated that a matrix fuel enrichment to 6.2% combined with uniform dispersion of 0.011 wt.% gadolinia (Gd_2O_3) as an integral burnable absorber (IBA) within the silumin matrix successfully matched the baseline operating lifetime of 846 effective full-power days (EFPD). Furthermore, the alternative fuel supported nonproliferation objectives by yielding a 3.1% reduction in total fissile content at end of cycle. The study demonstrates that the proposed UO_2-silumin cermet fuel delivers excellent heat-removal capabilities and equivalent fuel-cycle length performance, establishing it as a promising candidate for enhanced accident tolerance and fuel-element optimization in existing light water reactors.

*Corresponding author
Email Address: **rfmenorjr@pnri.dost.gov.ph**
Date received: 04 June 2026
Dates revised: 18 July 2026
Date accepted: 30 July 2026
DOI: https://doi.org/10.54645/202619SupANN-98

INTRODUCTION

The VVER-1200 is an advanced Generation III+ pressurized water reactor (PWR) design featuring enhanced passive safety systems, first commissioned commercially at the Novovoronezh II Nuclear Power Plant Unit 6 in 2016 (Asmolov et al. 2017). Like conventional commercial light water reactors (LWRs), its standard core configuration utilizes ceramic uranium dioxide (UO_2) fuel pellets enriched up to 5 wt.% ^{235}U, encased within a zirconium-based alloy cladding matrix (Bragg-Sitton 2012; Marguet 2022). This traditional fuel system has operated successfully for decades due to its favorable neutronic characteristics, structural stability, and predictable behavior during standard operating conditions. However, the intrinsic properties of ceramic UO_2, most notably its low thermal conductivity and accelerated high-temperature steam oxidation, substantially limit safety margins and accelerate core degradation under beyond-design-basis accident (BDBA) scenarios (Hofmann 1999; Rebak 2020).

Following the Fukushima Daiichi nuclear accident in 2011, global research initiatives redirected significant attention toward alternative fuel and cladding materials capable of providing enhanced safety margins and prolonged operator coping times under severe accident conditions. These systems are collectively classified as accident-tolerant fuels (ATFs) (Zinkle et al. 2014). As illustrated in Figure 1, international ATF development paths broadly encompass three main categories: alternative fuel materials, advanced cladding concepts, and improved non-fuel materials (Krejčí et al. 2020; Li et al. 2024; Zabirov et al. 2024).

KEYWORDS

VVER-1200, Accident tolerant fuel, GETERA, Silumin, Dispersion fuel, Cermet

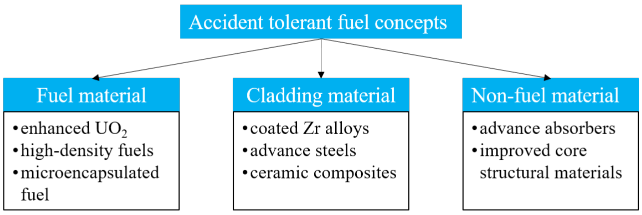

Figure 1: Classification of ATF concepts under development around the world.

Among alternative fuel geometries, composite fuels have shown significant potential for high-power density and elevated-temperature reactor deployment. A major subset of this type of fuel is cermet (ceramic-metallic) fuel, which consists of ceramic fuel particles uniformly dispersed within a continuous, non-fissile metallic matrix (Krishnaiah et al. 2003). Early experimental investigations into cermet ATFs in Russia evaluated fuel compositions utilizing 20 wt.% ^{235}U-enriched UO_2 particles embedded inside an aluminum-silicon (silumin) metal matrix (Baranaev et al. 2003; Popov et al. 1997). Currently, this specialized dispersion fuel technology is utilized within marine-based small modular reactors (SMRs), such as the RITM-200 design (IAEA 2020; Kulakov et al. 2020; Petrunin et al. 2019).

While its structural and thermal performance has been demonstrated in compact marine systems, the scalability, neutronic viability, and long-term isotopic transmutation behavior of UO_2-silumin cermet fuels in large-scale, high-power commercial reactors have not been characterized. To address this deficit, this study systematically evaluates the performance of a UO_2-silumin matrix fuel as a direct replacement for traditional UO_2 pellets within a VVER-1200 assembly. Using coupled modelling, this work evaluates and contrasts the steady-state core thermal-hydraulic parameters, burnup cycle limits, and the transient evolution of spent fuel isotopic and plutonium vector compositions.

MATERIALS AND METHODS

Reactor core description

The VVER-1200 features a rated thermal power of 3200 MW_{th} (yielding a net electrical output of approximately 1200 MW_e). The fully loaded reactor core is organized in a hexagonal lattice geometry containing 163 fuel assemblies (FAs). Each hexagonal fuel assembly consists of 312 active fuel rods, 18 control rod guide tubes, and 1 centrally located instrumentation tube. The detailed spatial layout of the hexagonal fuel pin array is illustrated in Figure 2 (Veretennikov et al. 2024). The complete thermal-hydraulic baseline conditions and structural geometrical parameters utilized to construct the computational model are consolidated in Table 1 (Dien and Diep 2017; IAEA 2021; Korotkikh and Odii 2025).

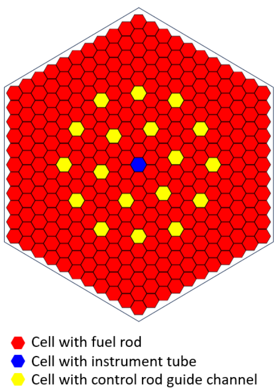

Figure 2: Cross-sectional layout of the hexagonal VVER-1200 fuel assembly.

Table 1: Operational parameters and core structural specifications of VVER-1200* reactor core.

Parameter	Value
Rated Thermal power, Q (MW_{th})	3200
Primary circuit operating pressure, P (MPa)	16.2
Coolant core inlet temperature, T_{in} (°C)	298.2
Coolant core outlet temperature, T_{out} (°C)	328.9
Steam generator pressure (MPa)	6.8
Feedwater temperature (°C)	227.0
Active core height, H (m)	3.75
Radial power peaking factor, K_r	1.39
Axial power peaking factor, K_z	1.53
Number of fuel assemblies, N_a	163
Number of fuel rods per assembly, N_f	312
Fuel rod pitch, s (mm)	12.75
Fuel assembly turnkey (mm)	235.1
FA shroud wall thickness (mm)	1.5
Fuel cladding outer diameter, d_{fc} (mm)	9.1
Fuel cladding wall thickness, δ (mm)	0.685
Fuel pellet outer diameter, d_f (mm)	7.6
Fuel pellet annular hole diameter, d_h (mm)	1.2
Number of control rod guide channel per assembly	18
Guide channel outer diameter (mm)	12.9
Number of instrumentation channel per assembly	1
Instrumentation channel outer diameter (mm)	12.9

*Operational parameters are based on VVER-1200(V-392M)

Reactor core materials

The reference VVER-1200 fuel configuration consists of ceramic UO_2 pellets enclosed within a zirconium-niobium alloy cladding. The reference ceramic pellet incorporates a central annular hole filled with helium gas (Figure 3a). The temperature-dependent thermal conductivity of the standard UO_2 is resolved using the empirical formulation proposed by Klimenko and Zorin (2003):

$$\lambda_{UO_2} = \frac{100}{7.5408 + 17.692 \cdot \tau + 3.6142 \cdot \tau^2} + \frac{6400}{\tau^{\frac{5}{2}}} \cdot \exp\left(-\frac{16.35}{\tau}\right), \frac{\mathrm{W}}{\mathrm{m \cdot K}} \quad (1)$$

where $\tau = \frac{\bar{T}}{1000}$, and $\bar{T}$ is the average fuel temperature in Kelvins.

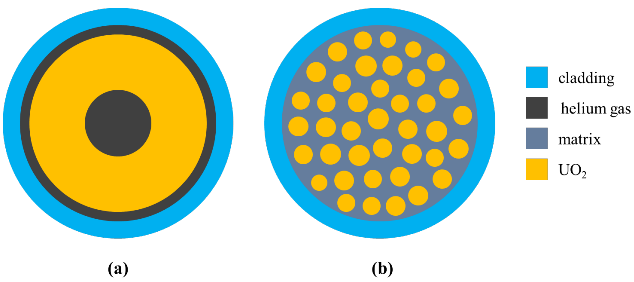

Figure 3: Radial schematic comparison of the fuel rod configurations: **a**) reference VVER-1200 annular pellet, and **b**) advanced homogeneous UO2-silumin cermet rod.

The alternative ATF modeled in this work is a cermet dispersion matching the fuel of the RITM-200 core. As shown in Figure 3b, inside the cladding, the fuel zone consists of UO_2 granules embedded within a low-porosity metallic silumin matrix. The fuel loading fraction is fixed at 66 wt.% UO_2 particles dispersed within 34 wt.% matrix (Savitsky and Kuzmin 2021). The thermal conductivity of silumin metal matrix varies according to Neimark (1967):

$$\lambda_m = 199.6 - 45 \cdot \tau, \frac{\mathrm{W}}{\mathrm{m \cdot K}} \quad (2)$$

To accurately predict the macro thermal conductivity of the composite UO_2-silumin fuel, Odelevskiy's formulation for multi-phase generalized conductivity is applied (Kushtym et al. 2017):

$$\lambda_{cermet} = \frac{(3\cdot V_m - 1)\cdot \lambda_m + (3\cdot V_{UO_2} - 1)\cdot \lambda_{UO_2}}{4} + \sqrt{\left(\frac{(3\cdot V_m - 1)\cdot \lambda_m + (3\cdot V_{UO_2} - 1)\cdot \lambda_{UO_2}}{4}\right)^2 + \frac{\lambda_m \cdot \lambda_{UO_2}}{2}}, \frac{W}{m\cdot K} \quad (3)$$

where V_{UO_2} and V_m represent the respective volume fractions of the embedded oxide granules and the metal matrix. Standard non-fuel core structural materials were modeled according to Russian specifications: Э-110 for the fuel cladding, 12X18H10T for the control rod guide tube, and Э-635 for the instrumentation guide tube.

Thermohydraulic analysis

To isolate and benchmark the fundamental heat transfer capabilities of the proposed UO_2-silumin cermet fuel against standard annular UO_2 fuel, the thermal-hydraulic analysis in this study was strictly constrained to steady-state conditions at the beginning-of-cycle (BOC).

While fuel performance over its burnup cycle is inherently dynamic, several time-dependent phenomena have been placed outside the scope of the current thermal evaluation. The helium-filled fuel-to-cladding gap was assumed to remain at its nominal initial thickness throughout the burnup cycle. The accumulation of fission gases and the resulting internal pin pressure buildup over the cycle were not calculated.

Conducting the thermal-hydraulic assessment at steady-state BOC provides a highly conservative "worst-case" baseline for thermal resistance. At BOC, the gas gap is at its widest (minimum gap conductance), and the helium fill-gas has not yet been diluted by lower-conductivity fission gases. This ensures that the calculated fuel centerline temperatures represent a conservative evaluation of the initial thermal safety margins of the cermet matrix.

Core thermal-hydraulic responses determine material temperatures for the subsequent neutronic transport calculations. The general scheme of this analytical approach traces the heat transfer mechanisms from the macroscopic reactor core down to the microscopic fuel pellet centerline as outlined by Korotkikh and Shamanin (2008). The variables, symbols, and units involved in this thermal-hydraulic scheme are summarized in Table 2.

Table 2: Nomenclature and variables used in the thermal-hydraulic calculation.

Symbol	Name	Unit
c_p	Heat capacity	J/(kg·K)
d	Diameter	mm
G	Coolant mass flow rate	kg/s
h	Enthalpy	J/kg
H	Core height	m
H_{eff}	Effective core height	m
K	Power peaking factor	
N_a	Number of fuel assembly	
N_f	Number of fuel rod	
P	Pressure	MPa
q_0	Linear heat flux	MW/m
Q	Thermal power	MW
R	Heat resistance	s^3·K/(kg·m)
s	Fuel rod pitch	mm
S_{fa}	Flow area	mm^2
T	Temperature	°C
z	Axial position	m
α	Heat transfer coefficient	W/(m^2·K)
δ	Cladding thickness	mm
λ	Thermal conductivity	W/(m·K)
Π	Wetted perimeter	mm

Subscript	Name
boil	boiling
c	coolant
cermet	UO_2-silumin fuel
conv	convective
crit	critical
f	fuel
fc	fuel cladding
g	gas gap
h	annular hole
hy	hydraulic
in	inlet coolant
onb	onset of nucleate boiling
out	outlet coolant
r	radial factor
s	saturated
UO_2	UO_2 fuel pellet
z	axial factor

The linear heat generation rate in the hottest core channel (q_0) was calculated via a homogeneous approximation method, which is suitable due to the symmetrical power distribution characteristic of PWRs:

$$q_0 = \frac{Q \cdot K_r \cdot K_z}{N_a \cdot N_f \cdot H} \quad (4)$$

The effective height is calculated below:

$$H_{eff} = K_z \cdot \sin\left(\frac{\pi \cdot H}{2 \cdot H_{eff}}\right) \quad (5)$$

Because the heat capacity of the coolant varies with temperature, the average integral heat capacity, calculated from energy considerations, is used:

$$c_p = \frac{h_{out} - h_{in}}{T_{out} - T_{in}} \quad (6)$$

where h_{in} and h_{out} indicate coolant enthalpies at the core inlet and outlet boundaries.

The bulk mass flow rate of the coolant through the active core zone (G) is computed from the overall core energy balance:

$$G = \frac{Q}{h_{out} - h_{in}} \quad (7)$$

The axial fluid temperature profile ($T_c(z)$) along the subchannel coordinate z bounded by $-H/2 \leq z \leq H/2$ is determined by integrating the heat flux distribution:

$$T_c(z) = T_{in} + \frac{N_a \cdot N_f}{G \cdot c_p} \cdot \int_{\frac{-H}{2}}^{z} q_0 \cdot \cos\left(\frac{\pi \cdot z}{H_{eff}}\right) dz \qquad (8)$$

Single-phase forced liquid convection heat transfer is resolved via the convective heat transfer coefficient:

$$\alpha_{conv} = \frac{Nu \cdot \lambda_c}{d_{hy}} \qquad (9)$$

where λ_c is the thermal conductivity of the coolant; d_{hy} is the hydraulic diameter calculated from the wetted parameter (Π) and flow area (S_{fa}) of one fuel assembly ($d_{hy} = 4 \cdot S_{fa}/\Pi$). For water-cooled rod bundles, the Nusselt number (Nu) is calculated using Subbotin's bundle correlation (Deev and Baisov 2021).

$$Nu = A \cdot \mathrm{Re}^{0.8} \cdot \mathrm{Pr}^{0.4} \qquad (10)$$

$$A = 0.0165 + 0.02\left(1 - \frac{0.91}{x^2}\right) x^{0.15} \qquad (10a)$$

where $x = s/d_{fc}$. The correlation is valid for $1.1 \leq x \leq 1.8$, $5 \cdot 10^3 \leq \mathrm{Re} \leq 5 \cdot 10^5$, and $0.7 \leq \mathrm{Pr} \leq 20$.

The onset of localized subcooled nucleate boiling occurs at the axial coordinate z_{onb} when the cladding outer surface temperature matches the saturation conditions (T_s). Beyond z_{onb}, the effective two-phase heat transfer coefficient (α) is resolved using Kutateladze's interpolation (Kutateladze 1961):

$$\alpha = \sqrt{(\alpha_{conv})^2 + (\alpha_{boil})^2} \qquad (11)$$

The fully developed pool boiling coefficient (α_{boil}) is calculated as a function of local pressure boundary states (Gorenflo and Kenning 2010):

$$\alpha_{boil} = B \cdot \left(\frac{q_0 \cdot cos\left(\frac{\pi \cdot z}{H_{eff}}\right)}{\pi \cdot d_{fc}}\right)^n \qquad (12)$$

$$n = 0.9 - 0.3 \cdot \left(\frac{P}{P_{crit}}\right)^{0.15} \qquad (12a)$$

$$B = 5600 \cdot \left(1.73 \cdot \left(\frac{P}{P_{crit}}\right)^{0.27} + \left(6.1 + \frac{0.68}{1 - \left(\frac{P}{P_{crit}}\right)^2}\right)\left(\frac{P}{P_{crit}}\right)^2\right)\left(\frac{1}{20 \cdot 10^3}\right)^n \qquad (12b)$$

where P_{crit} is the critical pressure of water. The resulting outer cladding wall surface temperature profile $T_{fc}(z)$ is mapped across both regimes:

$$T_{fc}(z) = \begin{cases} T_c(z) + \dfrac{q_0 \cdot cos\left(\frac{\pi \cdot z}{H_{eff}}\right)}{\pi \cdot d_{fc} \cdot \alpha_{conv}}, & -\dfrac{H}{2} \leq z \leq z_{onb} \\ T_s + \dfrac{1}{\alpha} \cdot \left(\dfrac{q_0 \cdot cos\left(\frac{\pi \cdot z}{H_{eff}}\right)}{\pi \cdot d_{fc}} - \alpha_{conv} \cdot \left(T_s - T_c(z)\right)\right), & z_{onb} \leq z \leq \dfrac{H}{2} \end{cases} \qquad (13)$$

The centerline temperature profile of the fuel $T_f(z)$ is solved by combining the conduction heat resistance profiles of the cladding (R_{fc}), gas gap (R_g), and fuel (R_f):

$$T_f(z) = T_{fc}(z) + q_0 \cdot \cos\left(\frac{\pi \cdot z}{H_{eff}}\right) \cdot \left(R_{fc} + R_g + R_f\right) \qquad (14)$$

$$R_{fc} = \frac{ln\left(\frac{d_{fc}}{d_{fc} - 2 \cdot \delta}\right)}{2 \cdot \pi \cdot \lambda_{fc}} \qquad (14a)$$

$$R_g = \begin{cases} \dfrac{ln\left(\frac{d_{fc} - 2 \cdot \delta}{d_f}\right)}{2 \cdot \pi \cdot \lambda_g}, & \text{traditional } \mathrm{UO_2} \text{ fuel} \\ 0, & \mathrm{UO_2} - \text{silumin fuel} \end{cases} \qquad (14b)$$

$$R_f = \begin{cases} \dfrac{1}{4 \cdot \pi \cdot \lambda_{UO_2}} \cdot \left(1 - \dfrac{2 \cdot \left(\frac{d_h}{2}\right)^2 \cdot ln\left(\frac{d_f}{d_h}\right)}{\left(\frac{d_f}{2}\right)^2 - \left(\frac{d_h}{2}\right)^2}\right), & \text{traditional } \mathrm{UO_2} \text{ fuel} \\ \dfrac{1}{4 \cdot \pi \cdot \lambda_{cermet}}, & \mathrm{UO_2} - \text{silumin fuel} \end{cases} \qquad (14c)$$

where the thermal conductivities of the cladding and helium gas are $\lambda_{fc} = 20 \frac{\mathrm{W}}{\mathrm{m \cdot K}}$ and $\lambda_g = 0.35 \frac{\mathrm{W}}{\mathrm{m \cdot K}}$, respectively.

Neutronic analysis

Neutronic multi-group transport calculations were carried out using the GETERA-93 code system. The GETERA-93 is a multi-group deterministic code that resolves the integral neutron transport equations across heterogeneous lattices via the first-collision probability method. In the slowing-down region (2.15 eV – 10.5 MeV), the neutron flux density is calculated using a 26-group approximation based on the BNAB-93 nuclear data library. In the thermalization region (0 – 2.15 eV) the code uses a special 100-group neutron cross-section library based on the ENDF/B-IV and JENDL-2 evaluated nuclear data files (Belousov et al. 1992). The accuracy of GETERA has been extensively benchmarked relative to other nuclear codes, including WIMS/WIMSD4 (Anisur and Uvakin 2019; Khattab and Dawahra 2011), MCNP4C/MCNPX (Abuqudaira and Stogov 2018; Dawahra et al. 2016), and SERPENT and MCU-PTR Monte Carlo codes (Aljasar et al. 2021).

While stochastic Monte Carlo codes are widely recognized for their high geometric fidelity, their application to iterative, multi-step burnup optimization problems carries a massive computational penalty. Monte Carlo methods rely on simulating billions of individual neutron histories to reduce statistical variance to acceptable levels. When tracking dozens of isotopic depletion steps over a full burnup cycle, a stochastic run can easily require days of wall-clock time on a computing cluster.

In this study, the deterministic lattice physics code GETERA-93 was selected specifically to exploit its high computational efficiency during the fuel design phase. By solving the integral transport equation, GETERA-93 completes a full, multi-step depletion sequence in less than a minute on a standard desktop workstation. All neutronic and depletion simulations in this study were executed on a localized workstation powered by an Intel(R) Core(TM) Ultra 5 125U processor (1.30 GHz with 12 cores and 14 threads) and equipped with 32.0 GB of RAM.

A homogenized cermet zone was utilized to represent the UO_2-silumin fuel mixture. Although studies on similar dispersion fuel systems using Monte Carlo methods have been reported, all employed a homogenized cermet model (Fajri et al. 2020; Hasan et al. 2026; Zhou et al. 2023).

The hexagonal VVER-1200 fuel assembly was modelled utilizing a reflective, infinite lattice polycell representation. In addition to zone-wise nuclide concentration, the parameters of the polycell strictly relating to VVER-1200 fuel assembly include the cell multiplicity, transition probability matrix for neutrons between individual monocells, and zone temperatures of the cells.

The material compositions, based on Deev et al. (2012), used in the neutronic analysis are detailed in Table 3. Mean material temperatures extracted from the preceding thermal-hydraulic calculation step were inputted into GETERA. Depletion trends of an average fuel assembly were executed at an average core power density of 108.5 MW/m^3 (Jamil and Ali 2024). The multiplication factor (k_∞) and fuel material compositions were tracked across sequential time intervals, with maximum step limits restricted to 100 days to preserve depletion accuracy.

Table 3: Material compositions and densities used in the neutronic model

Material	Description	Composition (wt. %)							
UO_2 10.4 g/cm^3	Standard fuel pellet	^{235}U 4.95	^{238}U 95.05						
Silumin 2.7 g/cm^3	Metal matrix*	Al 87	Si 11	Ni 2					
Э-110 6.5 g/cm^3	Fuel cladding	Zr 99	Nb 1						
12X18H10T 7.778 g/cm^3	Control rod guide tube	Fe 68.26	C 0.12	Si 0.80	Mn 2.00	Cr 18.00	Ni 10.00	Ti 0.8	S 0.02
Э-635 6.5 g/cm^3	Instrument guide tube	Zr 97.6	Nb 1.0	Sn 1.0	Fe 0.4				
Gd_2O_3 10.4 g/cm^3	Burnable absorber	^{155}Gd 14.8	^{156}Gd 69.55	^{157}Gd 15.65					

* For ATF UO2-silumin fuel composition, UO_2 particles are 66% by weight

Fuel optimization

The reference UO_2 assembly loading (4.95 wt.% ^{235}U) operated under a single-batch fuel reloading scheme and served as the baseline scenario. The assembly burnup was calculated until the end-of-cycle (EOC) transition, defined as the boundary where $k_\infty = 1$. This baseline set the benchmark operating cycle length in effective full-power days (EFPD).

To optimize the advanced ATF option, two bounding fuel cycle evaluations were first explored: an unoptimized replacement case utilizing the baseline enrichment (4.95 wt.% ^{235}U) and an upper bound utilizing a higher enrichment (20.0 wt.% ^{235}U) matching the enrichment bound of RITM-200 reactors. Within this bounded interval, an iterative interval-halving numerical search was executed. In each iteration, transport and depletion calculations were run in GETERA-93 to evaluate the EOC transition point. The search converged when the computed cycle length matched the baseline target within a tolerance of ±2 days.

Burnable absorbers must be introduced to manage elevated levels of initial excess reactivity. Traditional PWR methods use an integral burnable absorber (IBA) where gadolinia (Gd_2O_3) particles are mixed within selected fuel rods symmetrically distributed across the core. In this work, an alternative optimization approach was investigated: Gd_2O_3 was uniformly dispersed directly inside the silumin matrix across all 312 fuel rods in the assembly. Because the poison is distributed uniformly across all fuel rods rather than concentrated in a few discrete pins, the required concentration per unit volume is orders of magnitude lower than commercial oxide fuel baselines. The search algorithm incremented the Gd_2O_3 weight fraction in steps of 0.001 wt.% within the matrix. The optimal concentration was defined as the exact threshold where the peak multiplication factor aligns with the equilibrium xenon conditions of the standard UO_2 fuel.

RESULTS AND DISCUSSION

Steady-state thermal-hydraulic performance

The steady-state axial and radial temperature profiles computed along the hottest channel of the core are displayed in Figure 4. The fuel temperature profile shows a significant dependence on the fuel design. In Figure 4(a), the baseline UO_2 ceramic pellet displayed a steep thermal gradient, reaching a peak centerline temperature of 1819.7°C. In contrast, the UO_2-silumin fuel demonstrated lower temperatures, with its maximum centerline temperature reaching a maximum of 526.9°C. This represented an absolute decrease of 1292.8°C in peak fuel temperature. A noticeable difference in the radial temperature distributions is observed in Figure 4(b). For the annular ceramic UO_2 pellet, the maximum temperature was maintained across the central helium gas region ($r \leq 0.6$mm), whereas for the UO_2–silumin cermet fuel, the temperature decreases beyond the centerline.

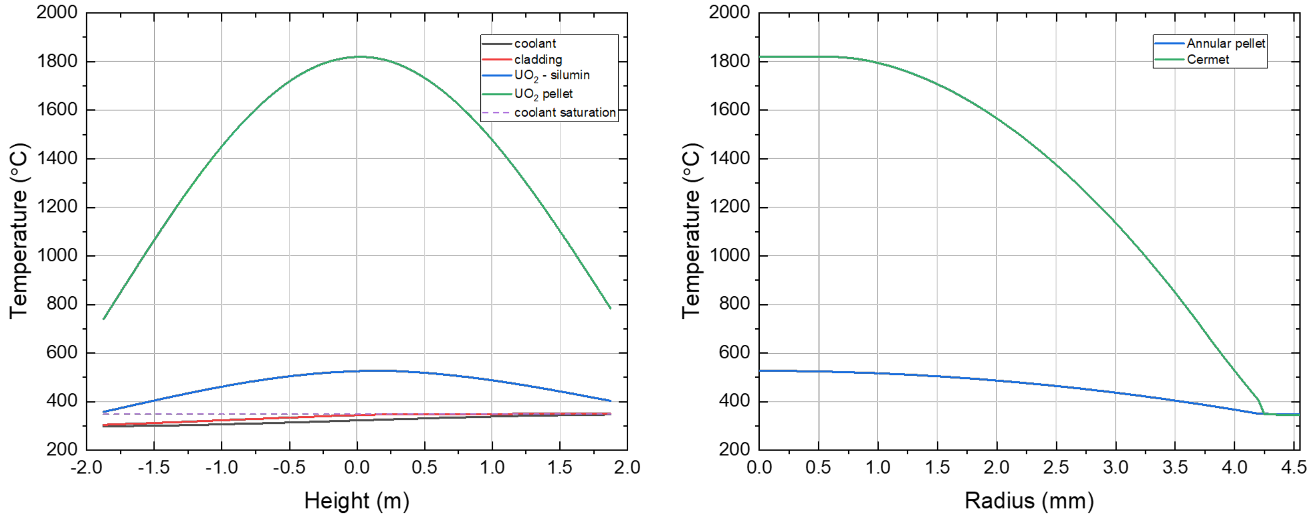

(a) **(b)**

Figure 4: Temperature profiles along (**a**) the axial direction of the fuel domains, cladding outer surface, and bulk coolant within the active core channel, and (**b**) the radial distribution of the two fuel types at their respective maximum axial temperatures.

This enhanced thermal behavior is primarily driven by two structural parameters: first, the high thermal conductivity of the UO_2-silumin cermet compared to the ceramic pellet; and second, the direct physical contact between the cermet and the cladding, which completely eliminates the thermal resistance R_g of the internal gas gap. While a standard helium gas gap is highly critical in conventional ceramic UO_2 fuel elements to accommodate high thermal expansion and progressive pressure buildup from thermal fission gas release, the UO_2-silumin cermet fuel's high thermal conductivity lowers the mean operating fuel temperature, thereby drastically reducing internal thermal stresses within the cermet fuel. Operating at substantially reduced mean fuel temperatures (471.2°C vs 1431.9°C) significantly enhances reactor safety margins by reducing core thermal energy and suppressing thermally driven fission gas release under high burnup conditions.

The calculated fuel centerline, fuel surface, and coolant temperatures, together with the mean temperatures used in GETERA-93, are summarized in Table 4.

Table 4: Maximum and mean temperatures of fuel, cladding, and coolant with corresponding peak locations

Material	Axial temperature Maximum (°C)	Location (m)	Mean (°C)
UO_2 pellet	1819.7	0.023	1431.9
UO_2-silumin	526.9	0.171	471.2
Outer cladding surface	349.7	1.623	336.7
Coolant	346.7	1.875	322.4

Neutronic analysis and cycle optimization

To characterize core behavior across different assembly loadings, the evolution of k_∞ was analyzed as a function of effective full-power days (EFPD). For the reference UO_2 assembly (4.95% enrichment), the BOC criticality peaked at 1.33164, stabilized at an equilibrium xenon condition of 1.28768, and reached its EOC depletion boundary at 846 days.

Figure 5 shows the depletion curves of the unoptimized and optimized advanced fuel alternatives contrasted against the baseline UO_2 burnup. When implementing the UO_2-silumin cermet at the baseline enrichment (4.95%), the unpoisoned BOC multiplication factor rose to 1.37396. This initial reactivity increase was a direct result of the dispersed-particle configuration, which reduced spatial self-shielding effects within the UO_2 granules and enhanced local neutron utilization. However, its operating lifetime was limited to only 660 days. This reduced operating cycle was caused by the lower volumetric density of uranium inside the composite cermet rod compared to a solid UO_2 pellet, resulting in a premature loss of criticality.

To extend core lifetime performance, an upper bounding evaluation was carried out using 20% enriched cermet matching RITM-200 limits. This configuration extended the core lifetime to 2507 days; however, it introduced a high BOC multiplication factor of 1.56204. Subsequent optimization iterations determined that a target enrichment of 6.2% is required to match the baseline cycle length of 846 EFPD. This optimized unpoisoned cermet fuel yielded a BOC k_∞ value of 1.41590.

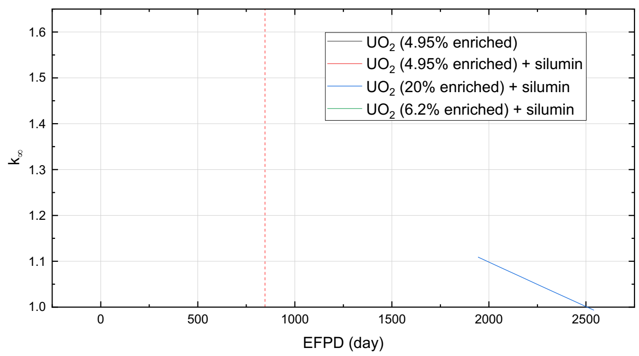

Figure 5: Multiplication factor evolution as a function of operational lifetime for various fuel configurations. The dotted vertical line indicates the baseline EOC of the standard UO_2 fuel.

To manage this initial excess reactivity, gadolinia burnable poisons were introduced directly into the silumin matrix. Figure 6 displays the reactivity suppression curve achieved through iterative simulations. Iterative increments of 0.001 wt.% identified the optimal Gd_2O_3 concentration as 0.011 wt.%, which established a suppressed peak criticality curve that closely matched the baseline UO_2 equilibrium xenon conditions. This demonstrates that matrix-dispersed burnable absorbers can successfully control the modified reactivity curves of cermet fuel types without compromising target fuel-cycle length performance.

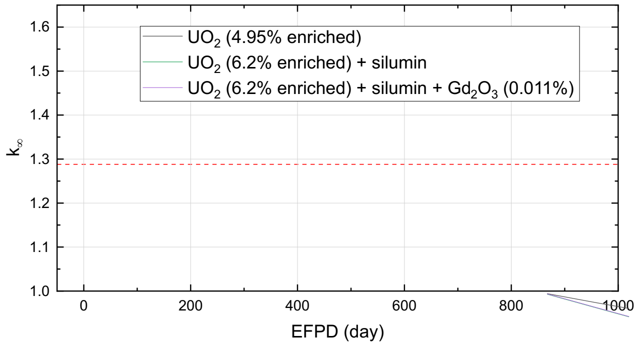

Figure 6: Suppression of excess reactivity in the optimized UO_2-silumin fuel via matrix-dispersed Gd_2O_3. The dotted horizontal line indicates the maximum criticality of the ATF fuel and the equilibrium xenon condition of the standard UO_2 fuel.

Spent fuel isotopic and plutonium vector evolution

Fuel burnup transitions involve the depletion of fissile ^{235}U and fertile ^{238}U alongside the generation of transuranic isotopes and fission products.

The isotopic depletion profiles of primary heavy metal isotopes ^{235}U and ^{238}U across the target operating cycle are compared in Figure 7(a) and (b), respectively. As shown in Figure 7(a), the initial concentration of ^{235}U in the cermet fuel was lower than that of the standard UO_2 fuel, despite the cermet's higher nominal enrichment of 6.2 wt.%. This behavior is driven by the volumetric dilution effect of the metallic silumin matrix. Because the metallic matrix displaces a fraction of the UO_2 granules within the pellet, the overall heavy metal loading density is reduced. This dilution is even more pronounced for the fertile ^{238}U isotope in Figure 7(b), where the cermet fuel's starting concentration was reduced to 1.44 $\times$ 10^{-2} atoms/(b·cm) compared to 2.08 $\times$ 10^{-2} atoms/(b·cm) in the standard fuel.

The transuranic transmutation profiles and the resulting generation of plutonium isotopes are shown in Figure 8. The comparative burnup profiles of the plutonium vectors exhibit distinct trends between the standard UO_2 and the UO_2-silumin cermet fuel forms. For the primary plutonium isotopes (^{239}Pu, ^{240}Pu, and ^{241}Pu), the standard UO_2 fuel maintained higher absolute concentrations throughout the burnup cycle. This behavior is attributed to the higher heavy metal loading of the pure UO_2 pellet, which provides a larger inventory of fertile ^{238}U; radiative neutron capture in ^{238}U accelerates ^{239}Pu breeding, subsequently feeding the sequential capture chain ($^{239}Pu \rightarrow {}^{240}Pu \rightarrow {}^{241}Pu$). At the beginning of the cycle, the concentration of ^{239}Pu rose rapidly in both fuels as the core established an equilibrium breeding balance. As the cycle progressed, the generation rate plateaued as ^{239}Pu began to contribute directly to the total core fission rate.

The concentrations of ^{238}Pu and ^{242}Pu were observed to be higher in the UO_2-silumin cermet fuel than in the reference fuel. The higher initial ^{235}U enrichment in the cermet fuel promotes neutron capture into the $^{236}U \rightarrow {}^{237}Np$ chain, leading to increased ^{238}Pu breeding. Furthermore, the matrix-diluted ^{238}U enhances localized resonance absorption, accelerating the transmutation pathway toward the heavier, terminal ^{242}Pu isotope and resulting in its higher concentration in the cermet fuel.

The spent fuel plutonium vector evaluations are summarized in Table 5. The findings reveal that the total fissile plutonium content (^{239}Pu + ^{241}Pu) in the spent fuel was 9.5 kg/ton of heavy metal (tHM) for the reference fuel and 8.5 kg/tHM for the optimized UO_2-silumin cermet fuel, representing an 11.2% reduction relative to the reference fuel. Concurrently, the ^{235}U content was 20.7 kg/tHM for the reference fuel and 20.8 kg/tHM for the optimized UO_2-silumin cermet fuel, representing a slight increase of 0.6% relative to the reference fuel. Summing all fissile heavy metal components, the spent reference fuel contained 30.3 kg/tHM, while the optimized UO_2-silumin fuel yielded 29.3 kg/tHM, representing a 3.1% reduction in fissile content in the spent fuel. This shifts the plutonium isotopic vector toward higher percentages of non-fissile isotopes (^{238}Pu, ^{240}Pu, and ^{242}Pu), which significantly increases the proliferation resistance of the spent fuel assemblies.

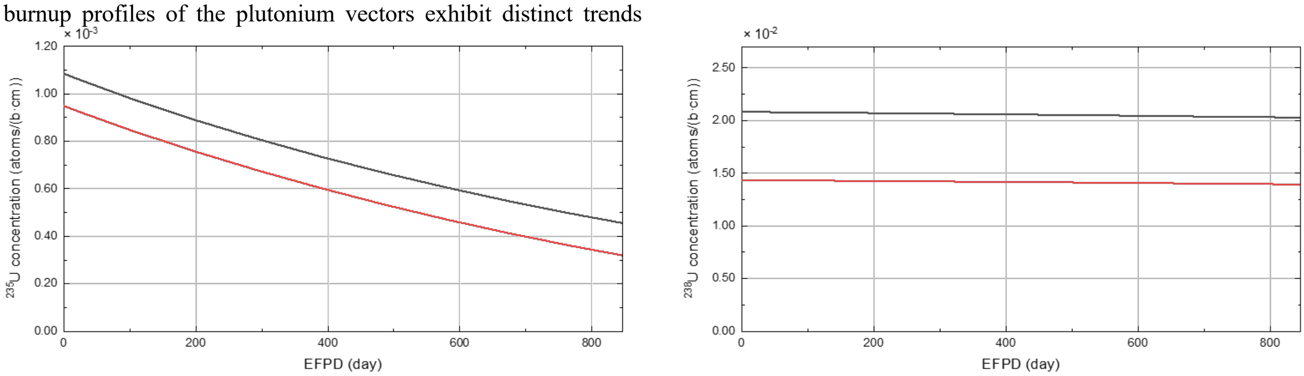

(a) **(b)**

Figure 7: Evolution of uranium isotope concentrations as a function of effective full power days (EFPD): (**a**) ^{235}U profile; (**b**) ^{238}U concentration profile.

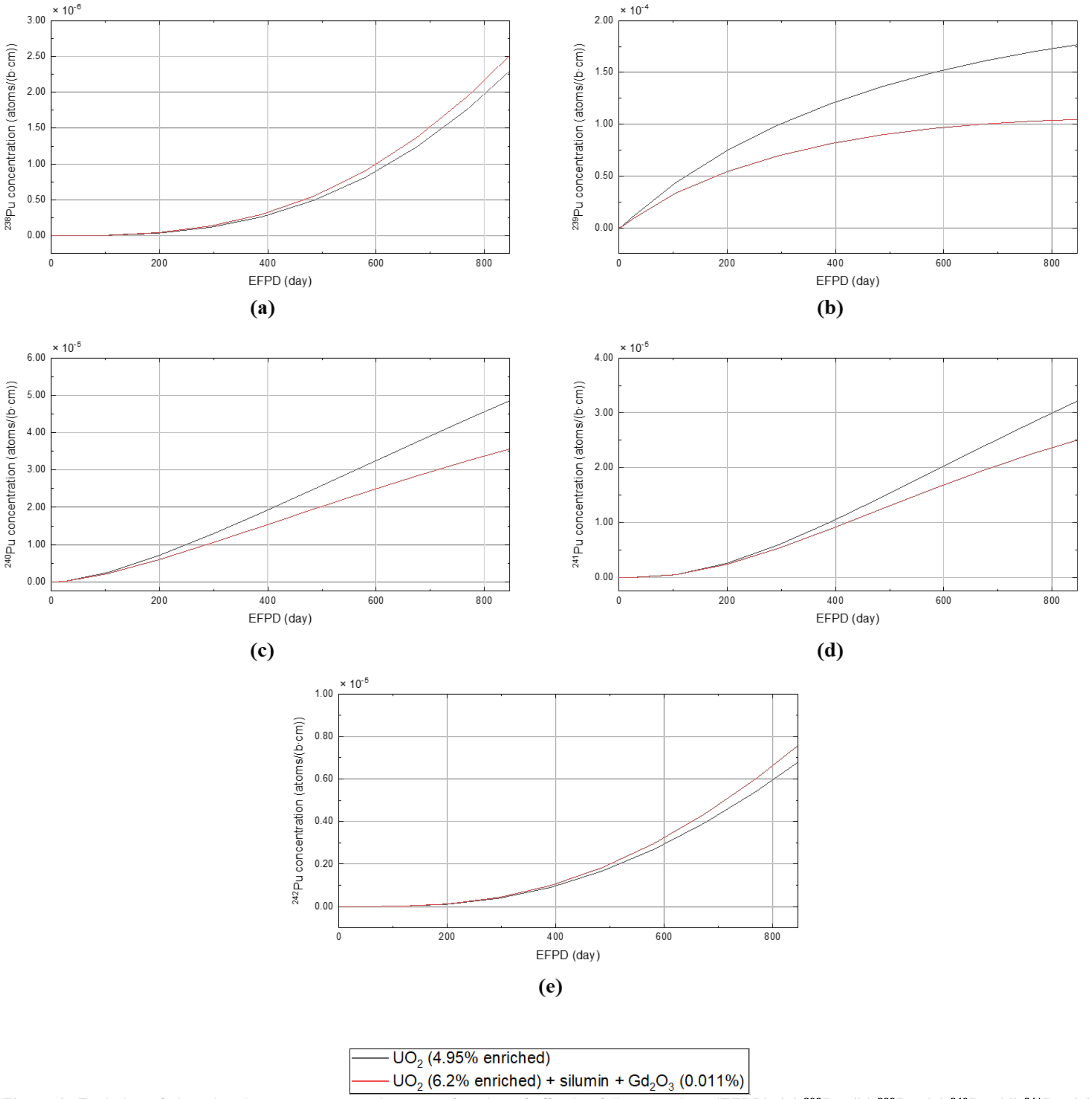

Figure 8: Evolution of plutonium isotope concentrations as a function of effective full power days (EFPD): (**a**) ^{238}Pu; (**b**) ^{239}Pu; (**c**) ^{240}Pu; (**d**) ^{241}Pu; (**e**) ^{242}Pu.

Table 5: Plutonium isotopic vectors at end of cycle for standard and alternative fuel

Isotope	Reference UO_2		Optimized UO_2-silumin fuel	
	Concentration (atoms/(b·cm))	%	Concentration (atoms/(b·cm))	%
^{238}Pu	2.2600×10^{-6}	0.9	2.5079×10^{-6}	1.4
^{239}Pu	1.7685×10^{-4}	66.3	1.0456×10^{-4}	59.7
^{240}Pu	4.8540×10^{-5}	18.2	3.5566×10^{-5}	20.3
^{241}Pu	3.2123×10^{-5}	12.0	2.5006×10^{-5}	14.3
^{242}Pu	6.7816×10^{-6}	2.5	7.5597×10^{-6}	4.3
Fissile plutonium content in the spent fuel, kg/ton of heavy metal	9.5		8.5	
Fissile uranium content in the spent fuel, kg/ton of heavy metal	20.7		20.8	
Total fissile content in the spent fuel, kg/ton of heavy metal	30.3		29.3	

CONCLUSION

This study conducted a coupled steady-state thermal-hydraulic and deterministic neutronic transport simulation analysis to evaluate the performance of an accident-tolerant UO_2-silumin cermet fuel as a direct candidate replacement within a commercial Generation III+ VVER-1200 reactor core.

The high thermal conductivity of the UO_2-silumin fuel paired with the complete elimination of internal rod gas gap resistance decreased the peak centerline fuel temperature from 1819.7°C to 526.9°C under normal operating conditions. This significantly expands thermal margin thresholds under severe core degradation events.

Increasing fuel enrichment to 6.2 wt.% ^{235}U successfully matched the target baseline operational cycle length of 846 effective full-power days. Incorporating 0.011 wt.% gadolinia burnable absorbers uniformly dispersed directly inside the silumin matrix successfully managed initial excess reactivity, matching equilibrium k_∞ trajectory of the baseline fuel.

Isotopic concentrations showed that the UO_2-silumin fuel reduced the fissile plutonium content by 11.2% while achieving a 3.1% net decrease in fissile material inside the spent nuclear fuel. This fuel shifted plutonium isotopes toward non-fissile isotopic fractions, significantly enhancing nonproliferation characteristics.

In summary, the proposed UO_2-silumin cermet fuel demonstrates excellent heat removal capability and comparable fuel-cycle performance, establishing it as a promising candidate for advanced fuel optimization and enhanced safety implementation in existing commercial light water reactors.

ACKNOWLEDGMENTS

The authors are grateful to the members of the Department of Science and Technology–Philippine Nuclear Research Institute (DOST-PNRI), Nuclear Reactor Operations Section, for their invaluable support and assistance throughout this work.

CONFLICT OF INTEREST

The authors declare that there is no conflict of interest.

USE OF AI

The authors declare that OpenAI GPT-5.5 Instant was used only to assist with language editing, grammar, readability, and text organization. All scientific content, including methodology, analysis, interpretation, and conclusions, was developed and verified by the authors. The authors take full responsibility for the accuracy and integrity of the work. No AI tools were used to generate, modify, or manipulate data, figures, or results.

CONTRIBUTIONS OF INDIVIDUAL AUTHORS

RF Menor Jr: Conceptualization, Methodology, Software, Data curation, Formal analysis, Writing. RS Hor: Conceptualization, Software, Data curation, Formal analysis, Writing.

REFERENCES

Abuqudaira TM, and Stogov YV. Neutronic calculations for the VVER-1000 LEU and MOX assembly computational benchmark using the GETERA code. Journal of Physics: Conference Series 2018; 1133(1). https://doi.org/10.1088/1742-6596/1133/1/012018

Aljasar SA, Naymushin AG, and Aish MM. Computational-Benchmark Analysis with the GETERA and SERPENT Softwares Tools for WWER Fuel Assemblies. Jilin Daxue Xuebao (Gongxueban)/Journal of Jilin University (Engineering and Technology Edition) 2021; 40(09–2021), 46–63. https://doi.org/10.17605/OSF.IO/JCNBS

Anisur RSK, and Uvakin MA. Compare the Result of Uncertainty Analysis in the Physical Calculations of WWER Cells in the Daily Maneuvering Schedule by GETERA and WIMS Programs. Глобальная Ядерная Безопасность 2019; 30(1), 90–100. https://doi.org/10.1088/1742-6596/1133/1/012048

Asmolov VG, Gusev IN, Kazanskiy VR, Povarov VP, and Statsura DB. New generation first-of-the kind unit – VVER-1200 design features. Nuclear Energy and Technology 2017; 3(4): 260–269. https://doi.org/10.1016/j.nucet.2017.10.003

Baranaev YD, Popov VV, Sharapov VN, and Troyanov VM. The feasibility of employing inert matrix ceramic fuels in a Russian light water reactor. Journal of Nuclear Materials 2003: 319, 154–158. https://doi.org/10.1016/S0022-3115(03)00211-3

Belousov N, Bichkov S, Marchuk Y, Prianichnikov A. Savander V, and Fyodorov I. The code GETERA for cell and polycell calculations models and capabilities. In: Proceedings of the 1992 Topical Meeting on Advance in Reactor Physics. American Nuclear Society, 1992: 2-516–2-523.

Bragg-Sitton SM. Light Water Reactor Sustainability Program. Advanced LWR Nuclear Fuel Cladding System Development Technical Program Plan. 2012.

Dawahra S, Khattab K, and Saba G. Calculation of fuel burnup and radioactive inventory in the CANDU reactor using the GETERA and MCNP4C codes. International Journal of Nuclear Energy Science and Technology 2016; 10(3), 183. https://doi.org/10.1504/IJNEST.2016.078956

Deev VI, and Baisov AM. Теплопередача в ЯЭУ (Heat Transfer in NPP). 2. Moscow, Russia:NRNU MEPhI, 2021.

Deev VI, Shchukin NV, and Cherezov AL. In: Deev VI, ed. Основы Расчета Судовых ЯЭУ: Учебное пособие (Fundamentals of Naval Nuclear Power Plant Calculations: Textbook). Moscow, Russia: NRNU MEPhI, 2012.

Dien LD, and Diep DN. Verification of VVER-1200 NPP Simulator in Normal Operation and Reactor Coolant Pump Coast-Down Transient. World Journal of Engineering and Technology 2017: 5(3), 507–519. https://doi.org/10.4236/wjet.2017.53043

Fajri DF, Agung A, and Harto AW. The Study of Floating Nuclear Power Plant Reactor Core Neutronic Parameters Using Scale 6.1 Code. International Journal on Advanced Science, Engineering and Information Technology.

2020;10(5):1774–1783. https://doi.org/10.18517/ijaseit.10.5.6609

Gorenflo D, and Kenning D. H2 Pool Boiling. In: VDI e. V., ed. VDI Heat Atlas. 2. Berlin, Heidelberg: Springer-Verlag Berlin Heidelberg, 2010:757–792.

Hasan MR, Rafi PM, Antor AR, and Ahmed MT. Comparative neutronic and radiotoxicity analysis of advanced nuclear fuels in a KLT-40S assembly. Kerntechnik. 2026;91(2):166–182. https://doi.org/10.1515/kern-2025-0095

Hofmann, P. Current knowledge on core degradation phenomena, a review. Journal of Nuclear Materials 1999; 270(1): 194–211. https://doi.org/10.1016/S0022-3115(98)00899-X

International Atomic Energy Agency (IAEA). Advances in Small Modular Reactor Technology Developments. Vienna, Austria:IAEA, 2020.

International Atomic Energy Agency (IAEA). Status report - VVER-1200 (V-392). 2021.

Jamil M, and Ali M. Fuel Performance Comparison of Uranium Nitride and Uranium Carbide in VVER-1200 using OpenMC. MATEC Web of Conferences. 2024;398:01008. https://doi.org/10.1051/matecconf/202439801008

Khattab K, and Dawahra S. Calculation of fuel burnup and radionuclide inventory in the Syrian miniature neutron source reactor using the GETERA code. Annals of Nuclear Energy 2011;38(6), 1442–1446. https://doi.org/10.1016/J.ANUCENE.2011.01.030

Klimenko AV, and Zorin VM. Тепловые и атомные электростанции: Справочник. Книга 3 (Thermal and Nuclear Power Plants: Handbook 3). Moscow, Russia: MEI Press, 2003.

Korotkikh, AG, and Odii CJ. Analysis of VVER-1200 thermal characteristics using analytical calculation validated by PCTran simulator. Discover Mechanical Engineering 2025: 4(79), 1–21. https://doi.org/10.1007/s44245-025-00175-7

Korotkikh AG, and Shamanin IV. Теплогидравлические процессы в ядерном реакторе и расчет их основных параметров (Thermal and hydraulic processes in a nuclear reactor and calculation of their main parameters). Tomsk, Russia:Tomsk Polytechnic University, 2008.

Krejčí J, Kabátová J, Manoch F, Kočí J, Cvrček L, Málek J, Krum S, Šutta P, Bublíková P, Halodová P, Namburi HK, and Ševeček M. Development and testing of multicomponent fuel cladding with enhanced accidental performance. Nuclear Engineering and Technology 2020; 52(3): 597–609. https://doi.org/10.1016/j.net.2019.08.015

Krishnaiah MV, Seenivasan G, Srirama Murti P, and Mathews CK. Thermal conductivity of selected cermet materials. Journal of Alloys and Compounds 2003; 353(1–2), 315–321. https://doi.org/10.1016/S0925-8388(02)01326-9

Kulakov GV, Vatulin AV, Ershov SA, Konovalov YB, Morozov AV, Savchenko AM, Sorokin VI, Romanov AI, Morozov OA, Shishin VY, and Sheldyakov AA. Разработка Топлива Для Атомных Станций Малой Мощности И Плавучих Энергоблоков, Состояние И Перспективы (Development of Fuel for Low Power Reactors and Floating Power Units. Status And Prospects). Вопросы Атомной Науки И Техники. Серия: Материаловедение И Новые Материалы 2020: 1(102), 116–128.

Kushtym AV, Belash MM, Zigunov VV, Slabospitska OO, and Zuyok VA. Dispersion fuel for nuclear research facilities. Problems of Atomic Science and Technology 2017; 108(2), 124–130.

Kutateladze SS. Boiling heat transfer. International Journal of Heat and Mass Transfer 1961: 4, 31–45. https://doi.org/10.1016/0017-9310(61)90059-X

Li Y, You E, Wang T, Xing D, Xu J, and Zhang H. Developments, challenges and prospects in thermal-hydraulic research on accident tolerant fuel. Heliyon 2024; 10(19), e38999. https://doi.org/10.1016/j.heliyon.2024.e38999

Marguet S. Fuel Management. The Technology of Pressurized Water Reactors: From the Nautilus to the EPR. France: Springer International Publishing, 2022: 1081–1084.

Neimark BE. Физические свойства сталей и сплавов, применяемых в энергетике: Справочник (Physical properties of steels and alloys used in the energy sector handbook). Leningrad: Energiya, 1967.

Petrunin VV, Fadeev YP, Pakhomov AN, Veshnyakov KB, Polunichev VI, and Shamanin IE. Conceptual Design of Small NPP with RITM-200 Reactor. Atomic Energy 2019: 125(6), 365–369. https://doi.org/10.1007/s10512-019-00495-4

Popov VV, Karpin AD, Isupov IA, Rumyantsev VN, Troyanov VM, Subonyaev VN, and Melnichenko NA. Results on experimental investigations for substantiation of WWER cermet fuel pin performance. In: International Atomic Energy Agency, ed. IAEA-TECDOC-970 Studies on Fuels with Low Fission Gas Release. Vienna, Austria:IAEA, 1997: 35–41

Rebak RB. Current materials in light water reactors. Why do we need a materials renewal?. Accident-Tolerant Materials for Light Water Reactor Fuels. Amsterdam, Netherlands: Elsevier, 2020: 15–41.

Savitsky DE, and Kuzmin AV. The calculation of the campaign of reactor RITM-200. IOP Conference Series: Materials Science and Engineering 14th International Forum on Strategic Technology (IFOST 2019) 2021: 1019(1). https://doi.org/10.1088/1757-899X/1019/1/012057

Zabirov AR, Molotova IA, Yagov VV, Sidelev DV, Yashnikov DA, and Shevchenko SA. Analysis of Thermophysical Justification of the Applicability of Accident Tolerant Fuel for Nuclear Power Plants: Current Concepts, Technologies, and Chemical Stability of Accident Tolerant Fuel. High Temperature 2024; 62(5): 669–696. https://doi.org/10.1134/S0018151X25700191

Zhou Z, Xie J, Deng N, Chen P, Wu Z, and Yu T. Effect of KLT-40S Fuel Assembly Design on Burnup Characteristics. Energies. 2023;16(8): 3364. https://doi.org/10.3390/en16083364

Zinkle SJ, Terrani KA, Gehin JC, Ott LJ, and Snead LL. Accident tolerant fuels for LWRs: A perspective. Journal of Nuclear Materials 2014; 448(1–3): 374–379. https://doi.org/10.1016/j.jnucmat.2013.12.005